Vietnam Journal of Earth Sciences, 42(4), 320–333, Doi: 10.15625/0866-7187/42/4/15281

(VAST)

Vietnam Academy of Science and Technology
Vietnam Journal of Earth Sciences
http://www.vjs.ac.vn/index.php/jse

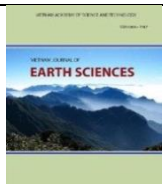

New observations of the total electron content and ionospheric scintillations over Ho Chi Minh city

Tam Dao[1*], Minh Le Huy[2], Brett Carter[1], Que Le[3,4], Thanh Thuy Trinh[3,4], Bao Ngoc Phan[3,4], Yuichi Otsuka[5]

[1]*SPACE Research Centre, School of Science, RMIT University, Australia*
[2]*Institute of Geophysics, VAST, Hanoi, Vietnam*
[3]*Department of Physics, International University, Ho Chi Minh City, Vietnam*
[4]*Vietnam National University, Ho Chi Minh City, Vietnam*
[5]*Institute for Space-Earth Environmental Research, Nagoya University, Nagoya, Japan*

Received 29 May 2020; Received in revised form 7 July 2020; Accepted 14 September 2020

ABSTRACT

In January 2018, a Trimble NetR9 GNSS receiver was installed at International University - Vietnam National University (IU-VNU), which is located at 10°52'N, 106°48'E in Ho Chi Minh City (HCMC). The GNSS signals recorded from ground-based receivers are useful for studying the ionospheric variations as well as the magnetosphere-ionosphere coupling effects, therefore, we aim to process and evaluate data recorded from this new station. Based on the obtained data, we first estimated the total electron content (TEC) using the carrier-phase method which is a combination of code and phase measurements. We then calculated the rate of change of TEC index (ROTI) with respect to time and investigated its day-to-day variations. Our results present typical features of diurnal and seasonal variations of TEC and ionospheric scintillation during 2018-2019. The distributions of ROTI over these two years of solar minimum show significant occurrences of scintillations, which are caused by small-scale ionospheric irregularities in the equatorial ionosphere. In addition, we found a significant increase of TEC in the latest strong geomagnetic storm in August 2018. The disturbance dynamo appears to have suppressed plasma bubbles after sunset and enhanced their formation at midnight. Thus, the disturbance dynamo effectively caused a delay of ionospheric scintillations. The TEC observed in HCMC also contributes to the data of ground-based observational receiver systems along 105°E longitude for studying ionospheric variations in low-latitude and equatorial regions. Our preliminary results indicate that the GNSS data collected at IU-VNU station is a valuable reference dataset for further research.

Keywords: GNSS receivers; Total Electron Content (TEC); the rate of change of TEC index (ROTI); geomagnetic storms; ionospheric scintillation.

1. Introduction

Global Navigation Satellite Systems (GNSS) currently include four global systems such as Global Positioning System (GPS), the Galileo, the GLONASS, and the Beidou. There are also two regional systems, which are the Quasi-Zenith Satellite System (QZSS)

*Corresponding author, Email: tam.dao@rmit.edu.au

and the Indian Regional Navigation Satellite System (IRNSS). With two frequencies in L-band, GNSS offers an excellent means to monitor and study the Earth's upper atmosphere.

The total electron content (TEC) is calculated along the ray path between the satellite and receiver by using the range delay of dual-frequency signals of GNSS satellites (Ciraolo, 1993 and reference therein). The variations of TEC and ionospheric variables are important for Satellite Based Augmentation System (SBAS) using differential wide area GPS technique since they cause a noticeable error on GNSS signals, especially in low latitude regions (Arenas, 2016). Ionospheric scintillations could also affect satellite communication, positioning and navigation systems.

The ionosphere is a partial plasma layer that ranges from 90 km to about 1000 km in the Earth's atmosphere. The electron density varies with height and maximizes around 400 km, at the altitude of the peak of *F*-layer (Kelly, 1989). The TEC recorded along the ray path of the GNSS satellite to the ground-based receiver mostly consists of electrons in the ionosphere. The plasmaspheric electron content also contributes to the measured TEC, but its contribution varies from about 10% at daytime and up to more than 50% at night (Lunt et al., 1999; Balan et al., 2002; Chen and Yao, 2015).

The capability of GPS receivers for studying regional equatorial ionospheric irregularities has been presented firstly by Aarons et al. (1996). After that, Pi et al. 1997 introduced an index based on TEC that shows the phase fluctuation of GPS signals being affected by ionospheric irregularities. The rate of changes of TEC index (ROTI) is defined as the standard deviation of the rate of change of TEC in 5-minute intervals, which can be used to characterize the seriousness of the GPS phase fluctuations and detect the presence of ionospheric irregularities as well as measure the irregular structures. ROTI reveals the presence of ionospheric irregularities on the scale of a few kilometres or more (Ma and Maruyama, 2003; Otsuka et al., 2004; Nishioka et al., 2008).

In the equatorial region, post-sunset depletion of electron density frequently occurs. These ionospheric features are so-called "plasma bubbles". Plasma bubbles reach up to approximately one hundred-kilometre scale-size and cause the loss-of-lock or ranging errors on the satellite signals. Until now, understanding and predicting day-to-day occurrence of plasma bubbles is still a challenging issue. Ionospheric irregularities with different scale sizes co-exist inside plasma bubbles (Basu et al., 1978; Otsuka et al., 2004; Dao et al., 2017). They are a major source of ionospheric scintillation. Therefore, the observational GNSS data can be used in coordination with other observations to conduct further study on forecasting plasma bubbles and scintillations.

The observations of TEC from GNSS receivers can contribute to understanding of the characteristics of ionospheric variations during geomagnetic storms. Since 1981, Kane observed the significant changes of TEC using the Faraday rotation method with data from a chain of low-latitude stations over India. Both positive and negative TEC enhancements were observed, but no clear relationships with either the specific phases or with the magnitude of the geomagnetic storms was identified. The responses of TEC in geomagnetic storms depend on latitudinal and longitudinal regions. Spogli et al. (2016) studied the formation of ionospheric irregularities over Southeast Asia during the St. Patrick's Day storm and confirmed a strong regional dependence on the storm development. Therefore, it is necessary to have a regional assessment in depicting the effect of geomagnetic storms. Investigating the responses of TEC and ionospheric

scintillations obtained in Vietnam to the geomagnetic storms have been conducted previously by using a single GPS station or continuous GNSS network (Dao T. and Duong V., 2013; Le Huy et al., 2016b). The TEC enhancements were often obtained depending on local time, while ionospheric scintillations were much correlated to solar activity and geomagnetic responses.

In this paper, we describe some features of a new GNSS receiver installed in HCMC. We then display the methods to calculate TEC and ROTI. Finally, we present some preliminary results of the variations of TEC and ROTI during two years of 2018-2019 and the responses of these parameters to a strong geomagnetic storm in August 2018.

2. A new GNSS receiver in Ho Chi Minh City (HCMC)

In the last two decades, tens of GPS/GNSS receivers have been installed along Vietnam for studying the ionosphere and space weather (Le Huy et al., 2006, 2016a). In HCMC, there was a GPS receiver installed at Hoc Mon which recorded data from 2006 to 2014 (Tran et al., 2017); it was then moved to Bac Lieu station. Installing a new GNSS reference station in this region has not only contributed to the ground-based ionospheric network in Vietnam, but also can be used for other purposes such as precise positioning and real-time kinematic measurement.

Within the memorandum of understanding between Centre for Spatial Information Science - University of Tokyo and International University - Vietnam National University, a Trimble NetR9 GNSS reference receiver was installed at IU-VNU (10°52'N, 106°48'E) in January 2018. The system offers advanced options for campaign Continuously Operating Reference Station (CORS). The receiver serves all common geodetic reference roles such as a campaign receiver or a permanent deployment. It makes a portable RTK base station with its internal battery or a reference receiver for scientific applications (http://navgeotech.com/ftp/user_guide/um_NetR9_en.pdf). Data are obtained every 1 second and 30 seconds continuously and are pushed onto the internet using an IP (internet protocol), such that we can access and download everywhere.

Station features:

- Station name: CREF0001,
- Station Code: IU-VNU,
- Correction controls for RTK (Real Time Kinematics) and DGNSS (Differential GNSS).

Antenna features:

- Type of Zephyr-Model 2 which minimizes multipath and offers robust low elevation tracking (can obtain data from 10° elevation).
- Weight of 0.64 kg; dimensions of 16.5 cm diameter × 7.6 cm height,
- Mounted stability in the top of an IU building (at height of 73 m).

The Trimble NetR9 is a multiple-frequency GNSS receiver. It includes 440-channels which can track all GNSS satellite signals in L-band such as GPS (L1/L2/L2C/L5), SBAS (L1/L5 supporting WASS, EGNOS and MSAS), GLONASS (L1 C/A and unencrypted P code, L2, and L3), Galileo (E1/E5), and QZSS (L1/L1-SAIF/L1C/L2C/L5).

Receiver features:

- 8 GB on-board storage,
- External USB drive support,
- Integrated battery, provides over 15-hour operation,
- Tracking and storage rates of up to 50 Hz,
- Ntrip (Networked Transport of RTCM via internet protocol) client/server/caster support.

The right side of Fig. 1 consists of some images of the antenna, the receiver, and a typical position map of different satellites (such as GPS, SBAS, GAL, QZSS) recorded at 16:40 UTC on 22 November 2019. On the left side of Fig. 1, location of the Trimble NetR9 GNSS in HCMC is shown by the blue dot, while the red

dots are twelve operating GNSS stations that we used to conduct the TEC map along 105°E longitude. The names and locations (longitude and latitude) of these stations are MLAY (103.154, 22.042), DBIV (103.018, 21.390), LSON (106.749, 21.853), PHUT (105.959, 21.030), QHOA (104.991, 20.525), CUSV (100.534, 13.736), DLAT (108.482, 11.945), HCMC (106.801, 10.878), BACL (105.711, 9.299), NTUS (103.680, 1.346), BAKO (106.849, -6.491), JOG2 (110.372, -7.737), and XMIS (105.684, -10.450).

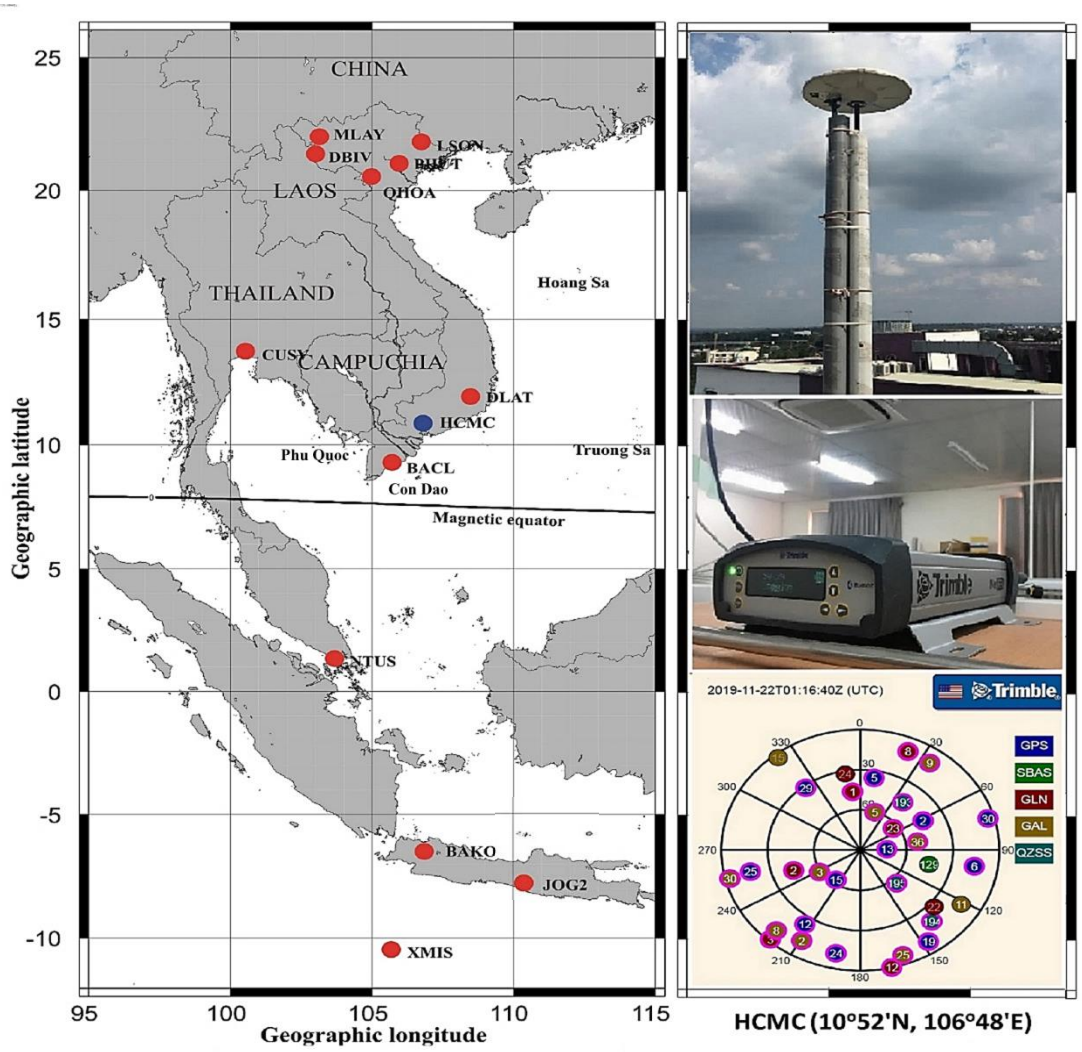

Figure 1. Location of GNSS receiver in HCMC (green dot in the left map), other red dots represent GPS/GNSS stations along 105°E longitude that we used to make TEC maps in this paper. Some images on the right side are the images of the antenna, receiver of the Trimble netR9 GNSS receiver, and position maps of different satellites (such as GPS, SBAS, GAL, QZSS) recorded at 16:40 UTC on 22 November 2019

3. Methodology for calculating TEC and ROTI

The TEC is the total number of electrons present along a path between a radio transmitter and receiver. These electrons will affect the radio signal when it passes through the electrons on its way, especially via the ionosphere. The total delay suffered by a radio

wave propagating through the ionosphere depends both on the frequency of the radio wave and the TEC between the transmitter and the receiver. TEC is measured in electrons per square meter, by convention, 1 TEC Unit (TECU) = 10^{16} electrons/m² (Klobuchar, 1983).

The GPS signals propagating through the ionosphere are delayed due to the total number of free electrons along the path of the signals from the satellite to the receiver. The carrier phase pseudo-ranges are measured to be too short and the code pseudo-ranges to be too long compared to the geometric range between the satellite and the receiver. Kumar et al. (2012) used the phase delay of L_1 and L_2 to derive TEC and found that 1 ns of differential time delay corresponds to 2.852 TECU.

In this paper, we use carrier-phase measurements between the GPS satellites and receiver to calculate the TEC along the transmission line (sTEC) to then construct the vertical TEC. Raw data obtained by the receiver as type of .T02 will be convert to RINEX (The Receiver Independent Exchange Format) file (https://kb.igs.org/hc/en-us/articles/201096516-IGS-Formats) which contains satellite numbers, pseudo-range and phase parameters. The details of the TEC calculation were presented in the paper of Le Huy et al. (2016b), which is briefly shown as follows:

$$sTEC = \frac{1}{40.3}\left(\frac{f_1^2 f_2^2}{f_1^2 - f_1^2}\right)\left[\left(L_1^i - L_2^i\right) - \left(b^i + b_\phi\right) - \left(\lambda_1 N_1^i - \lambda_2 N_2^i\right)\right], \quad (1)$$

where: f_1 = 1575.42 MHz and f_2 = 1227.60 MHz are GPS frequencies; L_1, L_2 are phase measurement from the i^{th} satellite to the receiver corresponding to the f_1 and f_2; N_1, N_2 are the multivalued integers; b^i is the instrumental bias of the i^{th} satellite and b_ϕ is the instrumental bias of the receiver.

From the equation of sTEC (1), for each receiver-satellite pair, sTEC is calculated as a combination of two terms:

$$sTEC_\Phi = \frac{1}{40.3}\left(\frac{f_1^2 f_2^2}{f_1^2 - f_2^2}\right)\left(L_{1,j}^i - L_{2,j}^i\right) \text{ and}$$

a $const = \frac{1}{40.3}\left(\frac{f_1^2 f_2^2}{f_1^2 - f_1^2}\right)\left[\left(b^i + b_\phi\right) + \left(\lambda_1 N_1^i - \lambda_2 N_2^i\right)\right.$.

$sTEC_\phi$ is derived from phase measurements, although while it is precise, it suffers spurious values/ "jumps" due to the cycle slips. These jumps could be estimated by comparison between $sTEC_\phi$ and $sTEC_p$ (sTEC from pseudo-range measurements) approximated by the fourth-degree polynomial on each satellite track.

The smoothed $sTEC_\phi$ is then converted to the vertical total electron content (TEC) observed at the pierce point of the ionosphere by using a single-layer model (Klobuchar, 1986).

$$TEC = sTEC_\Phi \cos\left[\arcsin\left(\frac{R\cos\theta}{R+h}\right)\right] \quad (2)$$

where θ is elevation angle in degrees; R is the mean radius of the Earth, h is the height of the ionosphere at the ionospheric pierce point. For our data processing, we use the average radius of the Earth R = 6371 km and the height of the single ionospheric layer h = 400 km. The vertical TEC obtained from (2) was compared with the vertical TEC from CODG model to determine the total delay of device delay and the non-determination of initial phase (const mentioned above). The error increases with increasing slant factor at lower elevation angle. Therefore, we excluded data with elevation angles less than 20° in further analysis.

Using the L_1 and L_2 phase measurements, we first calculate the rate of change of sTEC (ROT) with respect to time for each satellite-receiver pair as:

$$ROT = \frac{\Delta sTEC^i}{\Delta t}, \quad (3)$$

where: i is the visible satellite, t is the time of observation, Δt = 30s, and ROT is calculated in TECU/min.

ROT reveals the small-scale variations in the background of a larger-scale trend. This means that ROT varies if ionospheric irregularities occur on the ray path of satellite-receiver.

Then, we compute the rate of TEC change index (ROTI), which is defined as the standard deviation of ROT at a 5-minute interval.

$$ROTI = \sqrt{\langle ROT^2 \rangle - \langle ROT \rangle^2}\ . \quad (4)$$

The ROTI can be used to indicate the presence of scintillation-causing kilometre-scale ionospheric irregularities in the equator region (Pi et al., 1997). High ROTI value presents high scintillations of GPS signals transfer via the ionosphere.

For ionospheric scintillation analysis, we examine ROTI data with elevation angles lager than 10° by using a filter technique presented in Tran et al., 2017. Collecting low elevation angles from 10° can obtain more ionospheric scintillation over this station.

4. Observational results and Discussions

In this section, we present about preliminary results based on our observations during 2018-2019. It includes some typical features in the diurnal and seasonal variations of TEC, the possibilities of ionospheric scintillations observed by the rate of changes of TEC index, and responses of the ionosphere over HCMC station to a strong geomagnetic storm in 2018.

4.1. Typical features of TEC observed over HCMC

In 2018, solar activity was observed to be low as the end of solar cycle 24 approached. The yearly mean total sunspot number was as low as 7.0 (http://www.sidc.be/silso/datafiles). The daily vertical TEC observed over this station in 2018 is shown in Fig. 2. TEC is over 10 TECU in daytime during 0:00 to 13:00 UT (LT = UT+7), and the monthly TEC peaks reach from 20 to over 30 TECU. In night-time, TEC varies from 5 to 10 TECU.

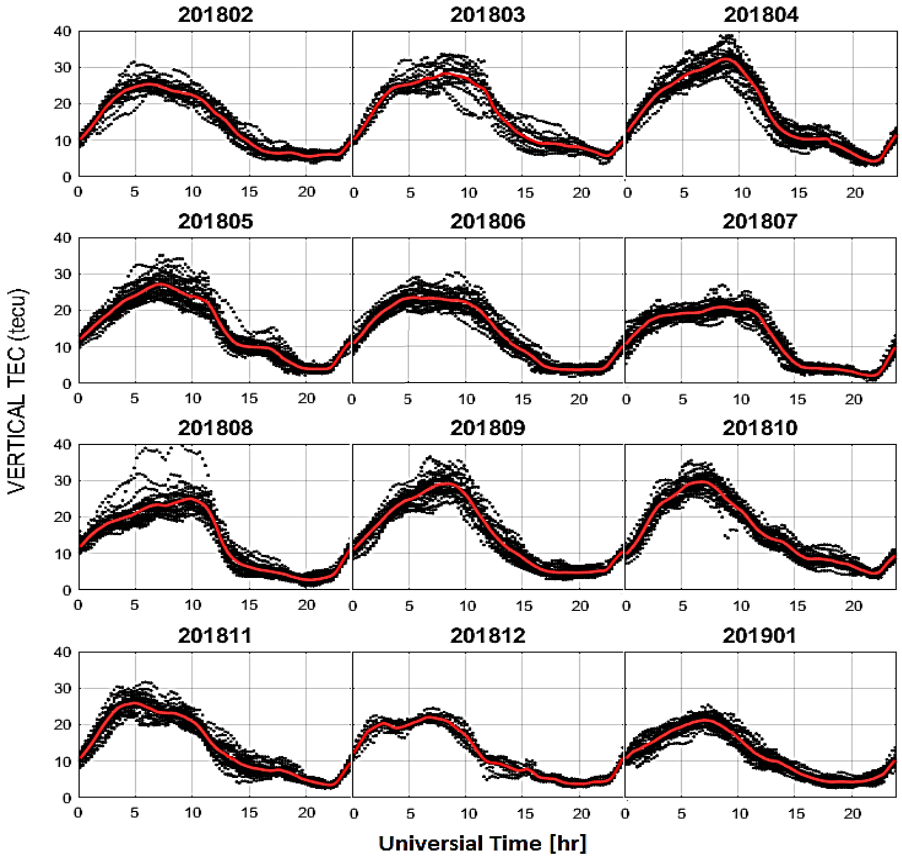

Figure 2. Daily and monthly vTEC variations observed in HCMC over one year from Feb 2018 to Jan 2019

The TEC observed every day collected during 2 years of 2018-2019 is presented in Fig. 3. This figure clearly shows diurnal and seasonal TEC distribution over HCMC. The daily TEC peak is around 7:00 UT (14:00 LT). High electron densities were observed around days 60-120 and 230-320 of the year, corresponding to March-April and September - October (equinoctial months). Lower TEC was observed in June - July and December - January (summer and winter time). The white areas indicate data gaps.

The high electron density in equinoxes and low electron density in summer and winter are consistent with observed TEC over the Southeast Asia region during the deep solar minimum 2008-2009 (Le Huy et al., 2014, 2016a). The seasonal variation of TEC is directly controlled by thermospheric neutral composition (Bagiya et al., 2009). During the daytime, meridional wind flows from the equator (the hotter place) towards the pole. This flow changes the neutral composition and increases the ratio of O/N_2 at equatorial and low latitude stations. This ratio is at its largest during equinoxes, resulting in higher electron density observed in equinoctial months (Titheridge, 1974).

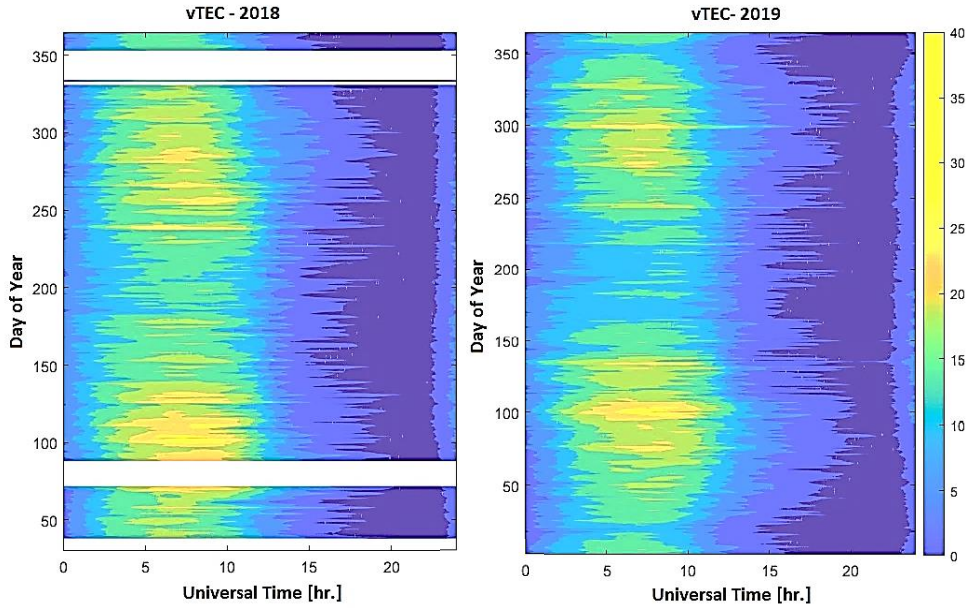

Figure 3. The vertical TEC retrieved in HCMC in 2018 and 2019 for all days of the year vs. universal time (UT). The colour in this figure shows TEC values in TECU with the levels shown in the colour bar

4.2. The rate of changes of TEC index (ROTI)

The variations of ionospheric range delay can be estimated by the change of total electron content along the receiver-satellite path. The rate of change of TEC index of each path in 5-min intervals presents the signal scintillations due to the ionosphere.

Figure 4 shows day-by-day variation of ROTI during the day of year 279 to 298 in October 2018. It is clearly shown that high ROTI occurred after 12 UT (19 LT) and lasted for 1 to 4 hours. These results are consistent with the S4 index observed in HCMC during 2006-2014 using GISTM receiver (Tran et al., 2011; 2015; 2017), which presented that most of the ionospheric scintillations occur after sunset until pre-midnight, from 19:00 to 24:00 LT, and the scintillations are maximum at about 20:00-21:00 LT.

Concerning the seasonal occurrence of high ROTI, we took the mean value of ROTI

with time for each day during 2018-2019 and plotted in Fig. 5. As shown in this Figure, there is a clear presence of high ROTI after 12 UT in equinoctial months, which corresponds well to the seasonal occurrence of plasma bubbles (Burke et al., 2004).

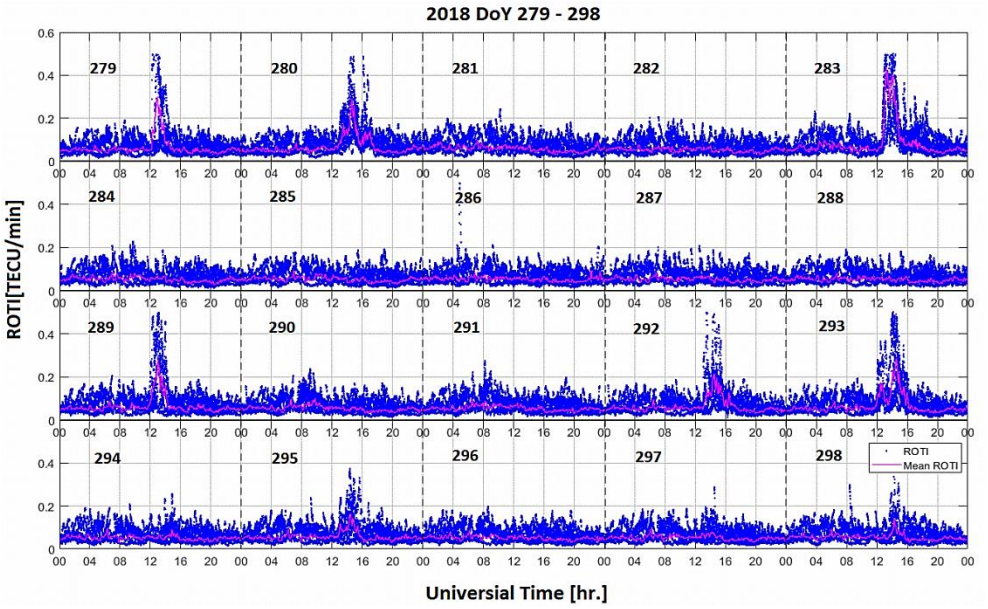

Figure 4. Day-by-day variability of ROTI during the day of 279-298 in 2018. Blue data points are ROTI along all satellite-receiver paths. The magenta line is the mean value calculated for all data points at the same time. The sudden increase of ROTI around 12-16 UT (20-23 LT) correlated to ionospheric scintillation at that time

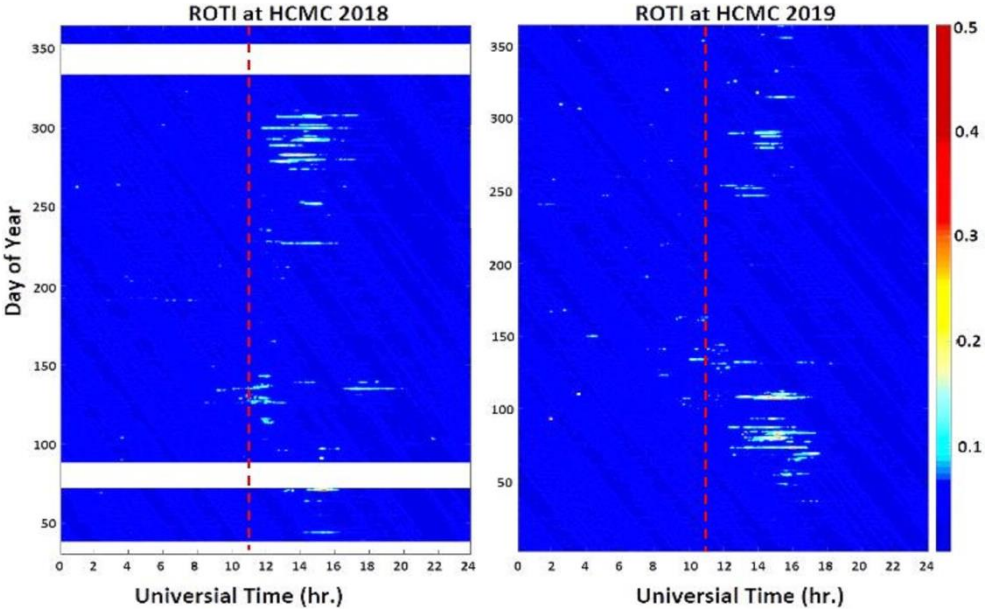

Figure 5. Variations of mean ROTI observed in HCMC over 2018-2019. The vertical dashed red lines represent to sunset time (18:00 LT). High ROTI is observed after sunset during equinoctial months

4.3. Case study of ionospheric responses on a strong geomagnetic storm

A surprising G3 geomagnetic storm that occurred in August 2018, during the period of low solar activity, can be examined to explore the effects of geomagnetic activity on the ionosphere above HCMC using observations from the GNSS receiver.

4.3.1. Geomagnetic conditions

On 21 August, a weak coronal mass ejection was detected by the SOHO/LASCO coronagraph imagery (https://www.swpc.noaa.gov/products/lasco-coronagraph). It looked like a minor filament eruption launched southwest of the Sun-Earth line aimed toward the Earth. Based on the solar wind data collected by the Deep Space Climate Observatory (DSCOVR) satellite shown in Fig. 6, the proton temperature on 21 August 2018 reached 10^6 K, the solar wind speed had increased to over 600 km/s and the dynamic pressure had a significant rise to more than 9.6 nPa during this day. The plasma cloud then created a significant change in the solar wind magnetic field. The southward orientation of magnetic field (Bz) was enhanced and persistently remained southward within the coronal mass ejection (magnetic cloud). The Bz had a negative value from around 15 UTC on August 25 and gradually decreased to the minimum of -18 nT which shows strongly southward directed solar wind magnetic field. The total magnetic field also reached nearly 20 nT in the morning of 26 August.

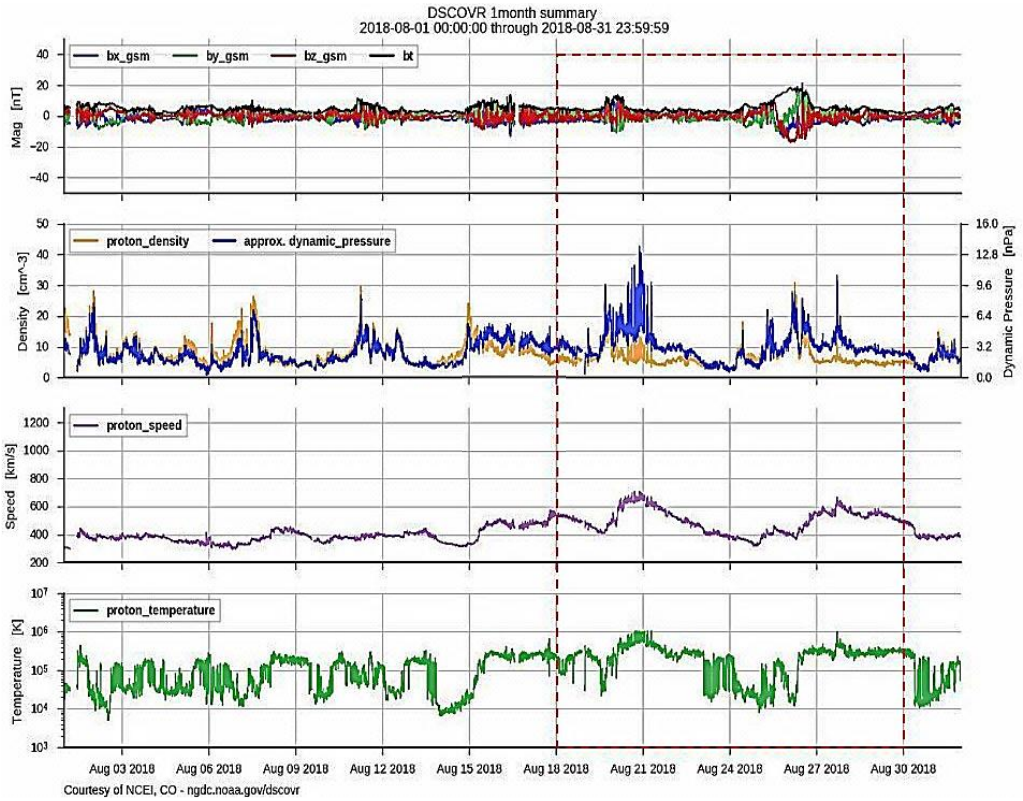

Figure 6. Intermedium data obtained from the satellite DSCOVR for the whole month of August 2018. The vertical dashed red box shows interesting data in for the magnetic storm event [https://www.ngdc.noaa.gov/dscovr/portal/index.html#/]

4.3.2. Responses of the ionosphere in the geomagnetic storm

The responses of the ionosphere observed using the GNSS receiver 24 to 29 August 2018 is presented in Fig. 7, which shows the variations of magnetosphere and ionosphere in this storm. Based on data recorded at WDC for Geomagnetism (http://wdc.kugi.kyoto-u.ac.jp/), the disturbance storm time index (Dst) dropped deeply to the lowest value of -174 nT at 7:00 UT on 26 August 2018 (Fig. 7b). In this event, the geomagnetic three-hour-range (Kp index) was at level 7 (Fig. 7c), reaching a strong (G3) geomagnetic storm threshold (https://spaceweather.sansa.org.za/space-weather-information/definitions/noaa-scales/297-geomagnetic-storm-scale).

In the row showing the vertical TEC (Fig. 7d), the blue line represents the monthly mean of TEC of quiet days in August and the red line describes the variation of TEC of each day during the storm. As shown in this figure, TEC has a strong increase during Aug 26. In this event, the CME reached the Earth during the day local Vietnam time, resulting in a TEC increase to a maximum of 185% in the main phase compared to the average TEC values. During the following days of the recovering phase, high TEC in daytime of two following days in the recovery phase was observed as 160% and 135% until it returned to pre-storm levels.

The increase of vertical TEC in the geomagnetic storm during the main phase can be explained by the high latitude convection electric field reaching the equatorial and low latitudes. This could relate to a southward ($Bz < 0$) and then northward turning of the z component of the interplanetary magnetic field (IMF-Bz) on 26 August (Fig. 7a). The sudden southward turning from a steady configuration produces a dawn to dusk convection electric field at high latitudes (Kikuchi et al., 1986; 2008).

Regarding ROTI variation in the storm, identical scintillations (ROTI>0.2 TECU/min) occurred repeatedly around sunset time (LT = 12UT+7) on the day of Aug. 24-26 (Fig. 7e). However, in the next day of the recovery phase, scintillations disappeared at 12 UT and occurred at night-time. The changing of scintillation time during the storm can be understood in terms of the disturbance dynamo electric field which is known to suppress the growth of plasma bubbles during the storm in the post-sunset sector and generate irregularities at midnight (Blanc and Richmond, 1980; Carter et al., 2016). In general, this geomagnetic storm occurred in low solar activity and during non-equinoctial months, therefore, scintillation conditions were already relatively weak. Piersanti et al. (2020) exploited data from both Low-Earth orbit satellites and more than 80 ground-based observatories located all over the world. They analysed the space-weather effects associated with this event and found no loss-of-lock during this strong geomagnetic storm.

Regarding the effect of disturbance dynamo in this geomagnetic storm, we examine the variations of TEC recorded by the GNSS network along 105°E longitude. Fig. 8 shows the latitudinal vs. UT variations of TEC during Aug 24-29, 2018. Data in these maps are collected from 13 GNSS stations in Vietnam and in Southeast Asian region. Names and locations of those stations are shown on the map of Fig. 1. The vertical TEC map by time and latitude in this figure has been smoothed by the method of running average of the overlapping windows, with the window size of 1h × 1°, the latitude sliding step is 0.75°, and the time slider is 0.75 hours. The temporal latitudinal TEC map has been introduced in previous articles (Le Huy et al., 2006; 2014; 2016a) which can be used to study the equatorial ionization anomaly (EIA). In this figure, TEC significantly increased on August 26 at all stations. The largest enhancement was at the northern crest, around 15-20°N, resulting in a TEC increase to over 200% of the average. In the main phase

of the storm, the southward Bz initiates a growth of substorm activity and a rapid increase of high-latitude convection. This brings a penetration of high-latitude convection electric fields into the low-latitude ionosphere (Kikuchi et al., 2008). Our data shows the northern EIA crest extended equatorward. After Bz turned northward and returned to normal states, the northern EIA tended poleward during the recovery phase.

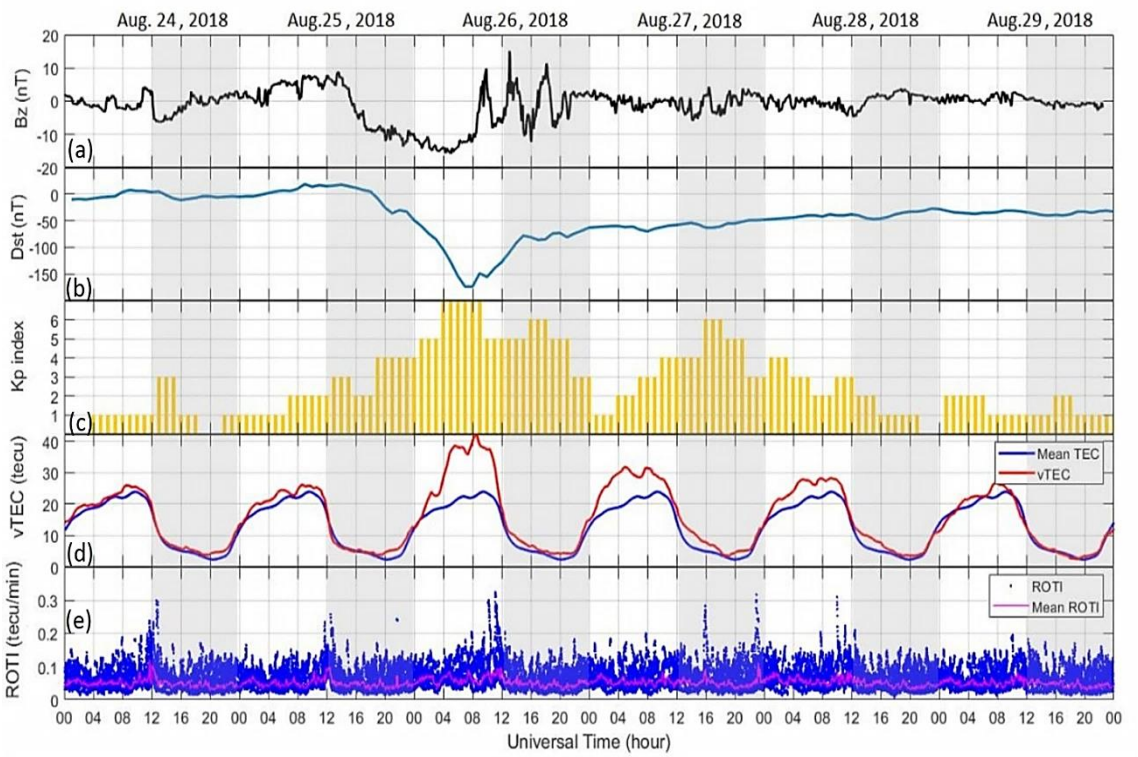

Figure 7. Bz, Kp, Dst and TEC, and ROTI variations in the G3 geomagnetic storm during August 24-29, 2018. The grey regions show the night local time

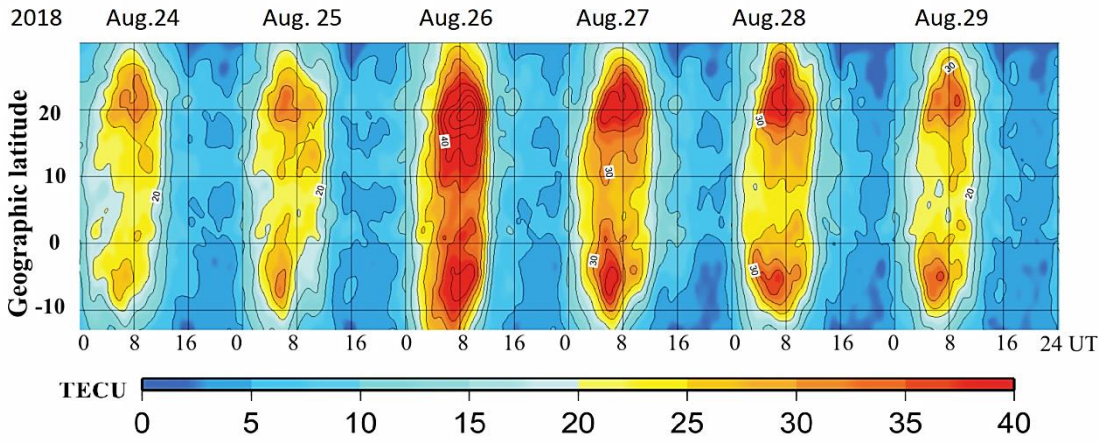

Figure 8. Vertical TEC variations collected from 13 low-latitude stations along 105°E longitude in the geomagnetic storm in August 2018. The level of contours is 5 TECU

5. Conclusions

Our study presents observational results of TEC recorded by a new GNSS station in HCMC. We observed the high TEC during equinoxes and the lowest TEC values during summer and winter time, which are in good agreement with previous studies.

Applying phase and pseudo-range methods to data obtained from IU-VNU station, we could observe high scintillation activities after sunset in equinox months during low solar activity years. The day-by-day occurrence of high ROTI is a useful tool for further investigations of ionospheric scintillations and plasma bubbles in this region, especially in the coming increasing solar activity.

A case study of a strong geomagnetic storm in August 2018 presents a positive change of TEC at all stations along 105°E longitude. In the main phase, TEC observed over HCMC increased to a maximum of 185% of the average TEC values and still enhanced in the recovery phase. During the recovery phase, post-sunset ionospheric scintillations appear to have been suppressed, while post-midnight scintillations appeared to be enhanced, indicating that the growth of plasma bubbles is suppressed after sunset and enhanced during post-midnight by disturbance dynamo effects.

Our results show that data recorded at IU-VNU station is good for estimating the total electron content to study ionospheric scintillations and geomagnetic storm effects. This station locates near the magnetic equator which is also useful for further research of ionospheric dynamics in conjunction with other observational techniques.

Acknowledgments

GNSS data collected in HCMC based on the joint research of International University - Vietnam National University and Centre for Spatial Information Science - Tokyo University. Support from the Australian Research Council (project LP160100561) is also acknowledged.

References

Aarons J., Mendillo M., R. Yantosca, 1996. GPS phase fluctuations in the equatorial region during the MISETA 1994 campaign. J. Geophys. Res., 101(A12), 26851–26862.

Arenas J., Sardón E., Sainz A., Ochoa B., Magdaleno S., 2016. Low-latitude ionospheric effects on SBAS, Radio Sci., 51, 603–618. Doi: 10.1002/2015RS005863.

Bagiya M.S., Joshi H.P., Iyer K.N., Aggarwal M., Ravindran S., Pathan B.M., 2009. TEC variations during low solar activity period (2005–2007) near the Equatorial Ionospheric Anomaly Crest region in India, Ann. Geophys., 27, 1047–1057. Doi.org/10.5194/angeo-27-1047-2009.

Balan N., Otsuka Y., Tsugawa T. Miyazaki S., Ogawa T., Shiokawa K., 2002. Plasmaspheric electron content in the GPS ray paths over Japan under magnetically quiet conditions at high solar activity. Earth Planets Space. 54, 71–79. Doi.org/10.1186/BF03352423.

Basu S., Basu S., Aarons J., Maclure J.P., Cousins M.D., 1978. On the coexistence of kilometer- and meter-scale irregularities in the nighttime equatorial F region, J. Geophys. Res., 83(A9), 4219–4226.

Blanc M., Richmond A., 1980. The ionospheric disturbance dynamo, J. Geophys. Res., 85, 1669–1686. Doi: 10.1029/JA085iA04p01669.

Burke W.J., Huang C.Y., Gentile L.C., Bauer L., 2004. Seasonal-longitudinal variability of equatorial plasma bubbles, Ann. Geophys., 22, 30893098.

Carter B.A., Yizengaw E., Retterer J. M., Francis M., Terkildsen M., Marshall R., Norman R., Zhang K., 2014. An analysis of the quiet-time day-to-day variability in the formation of post-sunset equatorial plasma bubbles in the Southeast Asian region, J. Geophys. Res. Space Physics, 119, 3206–3223. Doi:10.1002/2013JA019570.

Chen P., Yao Y., 2015. Research on global plasmaspheric electron content by using LEO occultation and GPS data. Adv Space Res, 55, 2248–2255. Doi: 10.1016/j.asr.2015.02.004.

Ciraolo L., 1993. Evaluation of GPS L2-L1 biases and related daily TEC profiles, in Proceedings of the GPS/Ionosphere Workshop, Neustrelitz, Germany, 90–97.

Dao T., Duong V., 2013. TEC and Scintillation observed over Ho Chi Minh City, Vietnam during 2009-2012. IEEE Xplore, IEEE International Conference on Space Science and Communication, July 1-3; Melaka, Malaysia, 434–439.

Dao T., Otsuka Y., Shiokawa K., Nishioka M., Yamamoto M., Buhari S.M., Abdullah M., Husin A., 2017. Coordinated observations of postmidnight irregularities and thermospheric neutral winds and temperatures at low latitudes, J. Geophys. Res. Space Physics, 122, 7504–7518. Doi: 10.1002/2017JA024048.

Kane R.P., 1981. Storm effects of ionospheric total electron content at low latitudes. J. Geomag. Geoelectr, 33, 399–409.

Kelley M.C., 1989. The Earth's Ionosphere. 1st edition: Academic Press, USA.

Kikuchi T., 1986. Evidence of transmission of polar electric fields to the low latitude at times of geomagnetic sudden commencements, J. Geophys. Res., 91, 3101–3105. Doi: 10.1029/JA091iA03p03101.

Kikuchi T., Hashimoto K.K., Nozaki K., 2008. Penetration of magnetospheric electric fields to the equator during a geomagnetic storm, J. Geophys. Res., 113, A06214. Doi: 10.1029/2007JA012628.

Klobuchar J.A., 1983. Ionospheric effects on Earth-space propagation, Environmental Research Papers, 866. Hanscom AFB: Air Force Geophysics Laboratory, AFGL-TR-84-0004.

Klobuchar J.A., 1986. Design and characteristics of the GPS ionospheric time-delay algorithm for single frequency users. In: Proceedings of PLAN'86: Position Location and Navigation Symposium, November 4-7; Las Vegas, Nevada. New York., 280–286.

Kumar S., Priyadarshi S., Gopi Krishna, Singh A.K., 2012. GPS-TEC variations during low solar activity period (2007–2009) at Indian low latitude stations, Astrophys Space Sci., 339, 165–178. Doi: Sanjay 10.1007/s10509-011-0973-6.

Le Huy M., Amory-Mazaudier C., Fleury R., Bourdillon A., Lassudrie-Duchesne P., L. Tran Thi, T. Nguyen Chien, T. Nguyen Ha, Vila P., 2014. Time variations of the total electron content in the Southeast Asian equatorial ionization anomaly for the period 2006-2011, Advances in Space Research, 54, 355–368. http://dx.doi.org/10.1016/-j.asr.2013.08.03.

Le Huy Minh, Bourdillon A., Lasudrie-Duchesne P., Fleury R., Nguyen Chien Thang, Tran Thi Lan, Ngo Van Quan, Le Truong Thanh, Hoang Thai Lan, Tran Ngoc Nam, 2006. Determination of the ionospheric total electron content in Vietnam through data of GPS stations, Journal of Geology, A269, 54–62.

Le Huy Minh, Tran Thi Lan, R. Fleury, C. Amory Mazaudier, Le Truong Thanh, Nguyen Chien Thang, Nguyen Ha Thanh, 2016a. TEC variations and ionospheric disturbances during the magnetic storm in March 2015 observed from continuous GPS data in the Southeast Asia region, Vietnam Journal of Earth Sciences, 38(3), 267–285.

Le Huy Minh, Tran Thi Lan, Amory-Mazaudier C., Fleury R., Bourdillon A., Hu J., Vu Tuan Hung, Nguyen Chien Thang, Le Truong Thanh, Nguyen Ha Thanh, 2016b. Continuous GPS network in Vietnam and results of study on the total electron content in the South East Asian region, Vietnam Journal of Earth Sciences, 38(2), 153–165.

Lunt N., Kersley L., Bishop G.J., Mazzella Jr. AJ., 1999. The contribution of the protonosphere to GPS total electron content: experimental measurements. Radio Sci., 34, 1273–1280, Doi: 10.1029/1999RS900016.

Ma G., Maruyama T., 2003. Derivation of TEC and estimation of instrumental biases from GEONET in Japan, Ann. Geophys., 21, 2083–2093. Doi: 10.5194/angeo-21-2083-2003.

Nishioka M., Saito A., Tsugawa T., 2008. Occurrence characteristics of plasma bubble derived from global ground-based GPS receiver networks, J. Geophys. Res., 113, A05301. Doi: 10.1029/2007JA012605.

Otsuka Y., Shiokawa K., Ogawa T., Yokoyama T., Yamamoto M., Fukao S., 2004. Spatial relationship

of equatorial plasma bubbles and field-aligned irregularities observed with an all-sky airglow imager and the Equatorial Atmosphere Radar, Geophys. Res. Lett., 31, L20802. Doi: 10.1029/2004GL020869.

Pi X., Mannucci A.J., Lindqwister U.J., Ho C.M., 1997. Monitoring of global ionospheric irregularities using the worldwide GPS network, Geophys. Res. Lett., 24(18), 2283–2286.

Piersanti, Mirko, De Michelis Paola, Del Moro Dario, Tozzi Roberta, Pezzopane Michael, Consolini Giuseppe, Marcucci Maria Laurenza, Monica, Di Matteo Simone, Pignalberi Alessio, Quattrociocchi Virgilio and Diego Piero, 2020. From the Sun to the Earth: August 25, 2018 geomagnetic storm effects. 10.5194/angeo-2019-165.

Spogli L., Cesaroni C., Di Mauro D., Pezzopane M., Alfonsi L., Musicò E., Povero G., Pini M., Dovis F., Romero R., Linty N., Abadi P., Nuraeni F., Husin A., Le H.M., Tran T.L., La T.V., Gil Pillat V., Floury N., 2016. Formation of ionospheric irregularities over Southeast Asia during the 2015 St. Patrick's Day storm. J. Geophys. Res. Space Physics, 121, 12211–12233.

Titheridge J.E, 1974. Changes in atmospheric composition inferred from ionospheric production rates. J. Atmos. Sol.-Terr. Phys., 36(7), 1249–1257.

Tran Thi Lan, Le Huy Minh, 2011. The temporal variations of the total electron content (TEC) and the ionospheric scintillation according to the continuous GPS data in Vietnam, Vietnam Journal of Earth Sciences, 33(4), 681–689.

Tran Thi Lan, Le Huy Minh, Amory-Mazaudier C., Fleury R., 2017. Climatology of ionospheric scintillation over the Vietnam low-latitude region for the period 2006-2014, Advances in Space Research, 60, 1657–1669.

Tran Thi Lan, Le Huy Minh, R. Fleury, Tran Viet Phuong, Nguyen Ha Thanh, 2015. The occurrence characteristics of the ionospheric scintillation in Vietnam in the period 2009-2012, Vietnam Journal of Earth Sciences, 37(3), 264–274.